ELSEVIER

Signal Processing 57 (1997) 177–194

SIGNAL PROCESSING

Adaptive beamforming with interpolated arrays for multiple coherent interferers

Ta-Sung Lee*, Tsui-Tsai Lin

Department of Communications Engineering, National Chiao Tung University, Hsinchu, Taiwan

Received 15 March 1996; revised 17 October 1996

Abstract

The spatial smoothing technique is effective in decorrelating multiple coherent interferers for an adaptive beamformer. However, it requires a configuration with identical subarrays. This paper presents an interpolation scheme to synthesize multiple virtual subarrays allowing for the use of spatial smoothing from a real array of arbitrary geometry. After interpolation, the optimum spatially smoothed subarray beamformer is constructed. A dimension recovery transformation can then be implemented to calculate the weights of the full array which will retain the interference nulls of the subarray beamformer. The efficacy of the proposed scheme is assessed through simulation. © 1997 Elsevier Science B.V.

Zusammenfassung

Allgemein stellt die Technik der räumlichen Glättung bei Verwendung eines adaptiven Beamformers ein effizientes Mittel dar, um mehrere kohärente Störquellen zu dekorrelieren. Allerdings wird hierbei eine Sensoranordnung benötigt, die aus identischen Sensorgruppen besteht. Dieser Artikel stellt ein Interpolationsverfahren vor, mit dessen Hilfe mehrere virtuelle Sensorgruppen synthetisiert werden können, so daß die räumliche Glättung auch bei Sensorgruppen beliebiger Geometrie angewandt werden kann. Nach der Interpolation wird der optimale räumlich geglättete Untergruppenbeamformer konstruiert. Anschließend kann eine Dimensions–Rückgewinnungstransformation implementiert werden, um die Gewichtsfaktoren für die gesamte Sensorgruppe zu berechnen. Dabei bleiben die Nullstellen im Diagramm des Untergruppenbeamformers an den Störpositionen erhalten. Abschließend wird die Wirksamkeit des vorgestellten Verfahrens anhand von Simulationen beurteilt. © 1997 Elsevier Science B.V.

Résumé

La technique de lissage spatial est efficace pour décorréler des signaux d'interférence multiples cohérents dans un formatteur de voie adaptatif. Toutefois, elle réclame une configuration comprenant des sous-réseaux identiques. Cet article présente une méthode d'interpolation pour synthétiser, à partir d'un réseau de géomètrie arbitraire, des sous-réseaux virtuels multiples permettant l'utilisation du lissage spatial. Après interpolation, le formatteur de voie optimal du sous-réseau lissé spatialement est construit. Une transformation de recouvrement de dimension peut ensuite être implantée afin de calculer les pondérations du réseau complet, qui conservera les zéros d'interférence du formatteur de voie du sous-réseau. L'efficacité du schéma proposé est montrée à l'aide de simulations. © 1997 Elsevier Science B.V.

Keywords: Beamforming; Array processing; Interpolation

* Corresponding author. Tel.: +886 35 712 121; fax: 886 35 710 116; e-mail: tslee@cc.nctu.edu.tw.

PII S0165-1684(96)00194-6

1. Introduction

An adaptive beamformer performs spatial filtering by forming a beam in such a fashion that the desired signal can be received with a large gain, while undesired interfering signals can be suppressed [6]. Conventional adaptive beamformers are found to be effective in suppressing strong interferers so long as the pointing error is negligible and the interferers are uncorrelated with the desired source. In the presence of pointing errors and/or correlated interferers, these beamformers exhibit degradation in performance in that the output signal-to-interference-plus-noise ratio (SINR) drops significantly. In some extreme cases, such as with large pointing errors or coherent interference, the conventional beamformers break down as a result of desired signal cancellation. Remedies have been proposed to lessen the effect of desired signal cancellation [3, 5, 11]. In particular, the Duvall processor was suggested in Ref. [11] as a means of improving the robustness of an adaptive beamformer operating on an array with the 'doublet' structure, such as the uniform linear array (ULA). With the Duvall processor, the desired signal is first attenuated by using a subtractive preprocessor. The optimum weights are then calculated based on the preprocessed data. With this mode of operation, the beamformer will not cancel the desired signal, even in the presence of pointing errors and coherent interference. We refer to this type of beamformers as the 'suppressed-desired signal' (SD) beamformers.

In spite of the success of dealing with pointing errors of moderate size and a single coherent interferer, the Duvall beamformer still exhibits a certain degradation in the presence of large pointing errors or multiple coherent interferers [3, 5, 7]. With large pointing errors, the desired signal cannot be attenuated sufficiently such that a portion of its power will be eliminated by the beamformer. This problem can be lessened by using high order look direction constraints to broaden the effective region of desired signal attenuation, or using some kind of algorithm to 'track' the desired source direction [3]. On the other hand, the difficulty incurred with multiple coherent interferers is a consequence of the fact that the relationship governing the mutual cancellation of the interfering signals in the master beamformer is destroyed in the slave beamformer. A similar situation which is likely to happen in a mobile scenario is that the relative phases of the coherent multipath signals change so rapidly that an adaptive beamformer is unable to keep up an effective mutual cancellation of these interferers. To avoid such degradation, the spatial smoothing technique [8] can be employed as a means of decorrelating the interferers before the optimum weights are obtained [4, 7, 8]. This ensures that the beamformer will suppress the interferers individually, instead of performing a mutual cancellation. However, working with spatial smoothing requires an array consisting of spatially shifted identical subarrays, which may not be attainable in practice. A question then arises as to whether an adaptive beamformer can be implemented on an arbitrary array to handle multiple coherent interferers. In [10], an interpolation technique was proposed for transforming an arbitrary array into a ULA such that spatial smoothing can be applied to estimate the directions of coherent sources. Detailed discussions on the interpolation procedure are given in Ref. [1]. It was shown that an interpolated array can perform almost as well as a real array for source localization [1]. Similar results can be expected for adaptive beamforming.

This paper presents a beamforming scheme for combating multiple coherent interferers with an interpolated array. The procedure consists of three steps. Firstly, spatially shifted identical virtual subarrays are synthesized from the same real array by linear interpolation [1]. Specifically, the interpolator is designed such that the interferers are transformed distortionlessly onto the virtual subarrays, whereas the desired source is eliminated. The latter operation is similar to the subtractive preprocessing in the Duvall beamformer. Secondly, a spatially smoothed virtual subarray correlation matrix is formed, from which the optimum weight vector can be obtained to produce a null for each interferer. Finally, the subarray weight vector is converted back into a full aperture weight vector acting on the real array via a dimension recovery transformation and post combining. Two different combiners are suggested: the maximum output signal-to-noise ratio (SNR) combiner and the eigen-based combiner. The former is easier to implement, whereas the latter is more robust to pointing errors. The efficacy of the proposed beamformer is ascertained by several sets of numerical examples using the nonuniform linear array and circular array configurations.

2. Problem formulation

2.1. Notations

$\mathbf{0}_n$	$n \times 1$ zero vector
$\|\cdot\|$	Euclidean norm
$E\{\cdot\}$	expectation
θ_d	desired source direction
θ_k	interfering source direction
θ_0	look direction
σ_n^2	noise power
γ	normalizing scalar
Θ	primary interpolation region
Θ_A	auxiliary interpolation region
Θ_D	interpolation region associated with desired signal
Θ_I	interpolation region associated with interference
ε	parameter controlling the relative emphasis between the interpolation performance over Θ and Θ_A
λ	wavelength
Φ_i	phase shift matrix associated with the ith subarray
$\phi_i(\theta)$	phase shift between the ith and reference subarrays for direction θ
γ_s	normalizing scalar
γ_g	normalizing scalar
ξ_i	generalized eigenvalue
$\Delta\theta$	deviation of interpolation region

Superscripts

T :	transpose
H :	complex conjugate transpose

2.2. Array model and beamforming

The scenario considered herein involves a single desired source and K possibly mutually correlated interferers, all assumed to be narrowband with the same center frequency. These sources are in the far field of an array consisting of M elements. Adopting the complex envelop notation, the array data obtained at a certain sampling instant can be put in the $M \times 1$ vector form:

$$\boldsymbol{x} = s_d\boldsymbol{a}(\theta_d) + \sum_{k=1}^{K} s_k\boldsymbol{a}(\theta_k) + \boldsymbol{n} = \boldsymbol{A}\boldsymbol{s} + \boldsymbol{n}, \tag{1}$$

where

$$\boldsymbol{A} = [\boldsymbol{a}(\theta_d), \boldsymbol{a}(\theta_1), \ldots, \boldsymbol{a}(\theta_K)], \tag{2}$$

and $\boldsymbol{s} = [s_d, s_1, \ldots, s_K]^T$. The random scalars s_d and s_k, $k = 1, \ldots, K$, represent the desired and interfering signal samples received at the reference point of the array. The $M \times 1$ vectors $\boldsymbol{a}(\theta_d)$ and $\boldsymbol{a}(\theta_k)$, $k = 1, \ldots, K$, are the direction vectors accounting for the gain and phase variations across the array due to the desired and interfering signals from direction θ_d and θ_k, $k = 1, \ldots, K$, respectively. Finally, the vector $\boldsymbol{n}$ is composed of the noise components present at the M elements. The noise is assumed to be spatially white with power σ_n^2 and uncorrelated with the desired and interfering signals.

A beamformer is a linear combiner which transforms the array data vector into a scalar y via an $M \times 1$ complex weight vector $\boldsymbol{w}$:

$$y = \boldsymbol{w}^H\boldsymbol{x}. \tag{3}$$

Associated with the beamformer constructed with $\boldsymbol{w}$ is the beam pattern defined by

$$w(\theta) = \boldsymbol{w}^H\boldsymbol{a}(\theta), \tag{4}$$

which describes the spatial response of the beamformer. The optimum beamformer which we will work with is constructed so as to minimize the output power subject to a unit response constraint in the look direction θ_0 :

$$\min_{\boldsymbol{w}} \quad E\{|y|^2\} \equiv \boldsymbol{w}^H\boldsymbol{R}_{xx}\boldsymbol{w}$$

$$\text{subject to} \quad \boldsymbol{w}^H\boldsymbol{a}(\theta_0) = 1, \tag{5}$$

where $\boldsymbol{R}_{xx}$ is the $M \times M$ data correlation matrix. Invoking the spatial whiteness of $\boldsymbol{n}$ and using (1), we have

$$\boldsymbol{R}_{xx} = E\{\boldsymbol{x}\boldsymbol{x}^H\} = \boldsymbol{A}\boldsymbol{R}_{ss}\boldsymbol{A}^H + \sigma_n^2\boldsymbol{I}_M, \tag{6}$$

where $\boldsymbol{R}_{ss} = E\{\boldsymbol{s}\boldsymbol{s}^H\}$ is the source correlation matrix, and $\boldsymbol{I}_M$ is the $M \times M$ identity matrix. The linearly constrained minimum variance (LCMV) problem [9] in (5) has the solution

$$\boldsymbol{w} = \gamma\boldsymbol{R}_{xx}^{-1}\boldsymbol{a}(\theta_0), \tag{7}$$

where γ is a normalizing scalar.

The optimum beamformer is known to perform poorly in the presence of pointing errors and/or coherent interference. A subtractive preprocessor can lessen the problem incurred with pointing errors and a single coherent interferer, but cannot handle multiple coherent interferers. This prompts the development of a scheme to decorrelate the interferers before beamforming. For an array consisting of identical subarrays, the decorrelation can be done with spatial smoothing. When this is not the case, one must resort to the numerical approach, i.e., array interpolation, to reconfigure the array.

3. Formation of the interpolated arrays

This section describes the procedure for forming the interpolated array and discusses various issues on array interpolation. The procedure involves creating L spatially shifted identical virtual subarrays of M_s elements from the real array.

3.1. Interpolation of virtual subarrays

There are two major considerations in designing the interpolated array. Firstly, both the configuration of the virtual subarrays and angular region for interpolation need be determined beforehand. Secondly, the original signal–noise condition should be retained on the interpolated array so as to ensure a reliable beamforming performance. In general, the virtual subarrays should have a similar 'shape' to that of the real array, and should span an overall aperture comparable to that of the real array so as to keep the interpolation error small. On the other hand, the size of each virtual subarray should be large enough to provide a sufficient degree of freedom for interference nulling. Nevertheless, the number of subarrays need not be large as the improvement in spatial smoothing benefited by a large L will be likely offset by the increased interpolation errors and computational complexity. To determine the angular region for interpolation, preliminary estimates of the source directions are necessary. They can be obtained by using a nonadaptive beamformer to scan over the spatial spectrum and locate the peaks. In order that the signal-noise condition does not change dramatically after interpolation, the source signals should be transformed distortionlessly and noise structure modified in a tolerable fashion. This issue will be discussed shortly.

The interpolation of virtual subarrays is performed in a linear fashion. That is, we use L transformation matrices $\boldsymbol{T}_i$, $i = 1,\ldots,L$, of size $M_s \times M$ to transform the real array direction vector $\boldsymbol{a}(\theta)$ into the virtual subarray direction vectors $\boldsymbol{b}_i(\theta)$, $i = 1,\ldots,L$, over a prescribed angular region Θ :

$$\boldsymbol{T}_i\boldsymbol{a}(\theta) = \boldsymbol{b}_i(\theta), \quad \theta \in \Theta, \ i = 1,\ldots,L. \tag{8}$$

Usually the interpolation region consists of several subregions around the hypothesized source directions obtained from the preliminary localization.

3.2. Suppressed-desired signal (SD) interpolators

As described earlier in Section 1, an effective way of avoiding desired signal cancellation due to pointing errors is to remove the look direction signal before beamforming. The idea can be incorporated into the interpolation process by forcing the transformed direction vectors to be zero in the neighborhood of the look direction. That is, we define the modified transformation matrices $\tilde{\boldsymbol{T}}_i$, $i = 1,\ldots,L$, such that

$$\tilde{\boldsymbol{T}}_i\boldsymbol{a}(\theta) = \begin{cases} \boldsymbol{0}_{M_s}, & \theta \in \Theta_D, \\ \boldsymbol{b}_i(\theta), & \theta \in \Theta_I, \end{cases} \quad i = 1,\ldots,L, \tag{9}$$

where we split Θ into $\Theta = \Theta_D \cup \Theta_I$, with Θ_D denoting the interpolation region associated with the desired source, and Θ_I the interpolation region associated with the interference. For brevity of notation, we rewrite (9) as

$$\tilde{\boldsymbol{T}}_i\boldsymbol{a}(\theta) = I_D(\theta)\boldsymbol{b}_i(\theta), \quad \theta \in \Theta, \ i = 1,\ldots,L, \tag{10}$$

where $I_D(\theta)$ is the indicator function defined by

$$I_D(\theta) = \begin{cases} 0, & \theta \in \Theta_D, \\ 1, & \theta \notin \Theta_D. \end{cases} \tag{11}$$

In general, the larger the angular region Θ_D over which the zero forcing is performed, the more robust the beamformer will be against pointing errors. In the following development, we will work with $\tilde{\boldsymbol{T}}_i$'s for beamforming and refer to them as the transformation matrices associated with SD type interpolator. The original form of $\boldsymbol{T}_i$'s will be employed later for the purpose of dimension recovery and will be referred to as the transformation matrices associated with regular type interpolator.

3.3. Solution of transformation matrices

Eqs. (8) and (9) do not hold in general, but can be approximated by the least-squares (LS) problems:

$$\min_{\boldsymbol{T}_i} \int_{\Theta} \|\boldsymbol{T}_i \boldsymbol{a}(\theta) - \boldsymbol{b}_i(\theta)\|^2 \, \mathrm{d}\theta \tag{12}$$

and

$$\min_{\tilde{\boldsymbol{T}}_i} \int_{\Theta} \|\tilde{\boldsymbol{T}}_i \boldsymbol{a}(\theta) - I_{\mathrm{D}}(\theta)\boldsymbol{b}_i(\theta)\|^2 \, \mathrm{d}\theta, \tag{13}$$

respectively, whose solutions are easily seen to be given by

$$\boldsymbol{T}_i = \int_{\Theta} \boldsymbol{b}_i(\theta)\boldsymbol{a}^{\mathrm{H}}(\theta) \, \mathrm{d}\theta \left[\int_{\Theta} \boldsymbol{a}(\theta)\boldsymbol{a}^{\mathrm{H}}(\theta) \, \mathrm{d}\theta\right]^{-1} \tag{14}$$

and

$$\tilde{\boldsymbol{T}}_i = \int_{\Theta} I_{\mathrm{D}}(\theta)\boldsymbol{b}_i(\theta)\boldsymbol{a}^{\mathrm{H}}(\theta) \, \mathrm{d}\theta \left[\int_{\Theta} \boldsymbol{a}(\theta)\boldsymbol{a}^{\mathrm{H}}(\theta)\mathrm{d}\theta\right]^{-1}, \tag{15}$$

respectively. These solutions may cause numerical problems if the interpolation region is small. In this case, the matrix $[\int_{\Theta} \boldsymbol{a}(\theta)\boldsymbol{a}^{\mathrm{H}}(\theta) \, \mathrm{d}\theta]^{-1}$ tends to be ill-conditioned, and the resulting transformation matrices in Eqs. (14) and (15) will have very large entries. This in turn results in an 'enlarged' virtual subarray noise correlation matrix as will be seen later in (35). As a result, the signal–noise condition will be dramatically distorted, and the beamformer may fail to eliminate the interferers since they are no longer the dominant sources.

The transformation matrices can be made better conditioned by augmenting Θ with an extra interpolation region Θ_{A} covering a much wider angular range. This leads to the modified problems corresponding to Eqs. (12) and (13):

$$\min_{\boldsymbol{T}_i} \int_{\Theta} \|\boldsymbol{T}_i \boldsymbol{a}(\theta) - \boldsymbol{b}_i(\theta)\|^2 \, \mathrm{d}\theta + \varepsilon \int_{\Theta_{\mathrm{A}}} \|\boldsymbol{T}_i \boldsymbol{a}(\theta) - \boldsymbol{b}_i(\theta)\|^2 \, \mathrm{d}\theta \tag{16}$$

and

$$\min_{\tilde{\boldsymbol{T}}_i} \int_{\Theta} \|\tilde{\boldsymbol{T}}_i \boldsymbol{a}(\theta) - I_{\mathrm{D}}(\theta)\boldsymbol{b}_i(\theta)\|^2 \, \mathrm{d}\theta + \varepsilon \int_{\Theta_{\mathrm{A}}} \|\tilde{\boldsymbol{T}}_i \boldsymbol{a}(\theta) - \boldsymbol{b}_i(\theta)\|^2 \, \mathrm{d}\theta, \tag{17}$$

where ε is a parameter controlling the relative emphasis between the interpolation performance over the primary (Θ) and auxiliary (Θ_{A}) regions. Accordingly, the resulting solutions are given by

$$\boldsymbol{T}_i = \left[\int_{\Theta} \boldsymbol{b}_i(\theta)\boldsymbol{a}^{\mathrm{H}}(\theta) \, \mathrm{d}\theta + \varepsilon \int_{\Theta_{\mathrm{A}}} \boldsymbol{b}_i(\theta)\boldsymbol{a}^{\mathrm{H}}(\theta) \, \mathrm{d}\theta\right] \boldsymbol{P}_{\varepsilon}^{-1} \tag{18}$$

and

$$\tilde{\boldsymbol{T}}_i = \left[\int_{\Theta} I_{\mathrm{D}}(\theta)\boldsymbol{b}_i(\theta)\boldsymbol{a}^{\mathrm{H}}(\theta) \, \mathrm{d}\theta + \varepsilon \int_{\Theta_{\mathrm{A}}} \boldsymbol{b}_i(\theta)\boldsymbol{a}^{\mathrm{H}}(\theta) \, \mathrm{d}\theta\right] \boldsymbol{P}_{\varepsilon}^{-1}, \tag{19}$$

where

$$\boldsymbol{P}_{\varepsilon} = \int_{\Theta} \boldsymbol{a}(\theta)\boldsymbol{a}^{\mathrm{H}}(\theta) \, \mathrm{d}\theta + \varepsilon \int_{\Theta_{\mathrm{A}}} \boldsymbol{a}(\theta)\boldsymbol{a}^{\mathrm{H}}(\theta) \, \mathrm{d}\theta. \tag{20}$$

3.4. Issues on interpolation process

Augmenting the interpolation region with Θ_{A} in Eqs. (18) and (19) will not only alleviate the ill-condition problem, but also improve the robustness of the transformation against errors in choosing the interpolation region. Of course, the improvement depends on the value of ε. In general, the larger ε is, the more robust the transformation will be, but the interpolation performance over Θ will be poorer. The opposite is true for a small ε. It appears that the selection of ε is an empirical and scenario dependent task requiring some trial-and-errors. In our experience, we found that the configurations of the real array and virtual subarrays are the dominant factors in the task. With the array configurations given, ε can be determined as that yielding an interpolation error below some prespecified threshold over Θ, and sufficiently stable over Θ_{A}. By performing the same trial for different combinations of Θ and Θ_{A}, an empirical rule for choosing the best ε value can be obtained. In fact, we have observed from simulations that the interpolation regions do not affect ε much, as long as they are of moderately small size.

As mentioned before, the primary interpolation region Θ must be determined beforehand by some kind of localization methods, such as spatial spectrum

search, to obtain coarse estimates of the source directions. There are other techniques which use initial estimates of source directions to overcome the drawbacks of conventional adaptive beamformers [3, 12]. Compared to these techniques, the advantage of the proposed one working with interpolated arrays lies in its robustness against errors in the initial localization process, or small variations of the source scenario. This will be demonstrated shortly in the simulation section. In a nonstationary environment, it is necessary to keep track of the sources by performing the localization process periodically to update the interpolation region. In this case, the transformation matrices and weight vectors must be updated accordingly.

3.5. Numerical examples

We here give numerical examples demonstrating the efficacy of the above described schemes. For performance evaluation, we define the total and local relative interpolation errors (TRIE and LRIE) as follows. For regular type:

$$\mathrm{TRIE} = \frac{1}{L}\sum_{i=1}^{L}\frac{\int_{\Theta}\|\boldsymbol{T}_i\boldsymbol{a}(\theta)-\boldsymbol{b}_i(\theta)\|^2\,\mathrm{d}\theta}{\int_{\Theta}\|\boldsymbol{b}_i(\theta)\|^2\,\mathrm{d}\theta},$$

$$\mathrm{LRIE} = \frac{1}{L}\sum_{i=1}^{L}\frac{\|\boldsymbol{T}_i\boldsymbol{a}(\theta)-\boldsymbol{b}_i(\theta)\|^2}{\|\boldsymbol{b}_i(\theta)\|^2}.$$

For SD type:

$$\mathrm{TRIE} = \frac{1}{L}\sum_{i=1}^{L}\frac{\int_{\Theta}\|\tilde{\boldsymbol{T}}_i\boldsymbol{a}(\theta)-I_{\mathrm{D}}(\theta)\boldsymbol{b}_i(\theta)\|^2\,\mathrm{d}\theta}{\int_{\Theta}\|\boldsymbol{b}_i(\theta)\|^2\,\mathrm{d}\theta},$$

$$\mathrm{LRIE} = \frac{1}{L}\sum_{i=1}^{L}\frac{\|\tilde{\boldsymbol{T}}_i\boldsymbol{a}(\theta)-I_{\mathrm{D}}(\theta)\boldsymbol{b}_i(\theta)\|^2}{\|\boldsymbol{b}_i(\theta)\|^2}.$$

In the first example, the array employed was a nonuniform linear array consisting of $M = 24$ identical omnidirectional elements with the following interelement spacings:

$$\{0.28\lambda, 0.28\lambda \times 1.05, 0.28\lambda \times 1.05^2, \times\ldots, 0.28\lambda \times 1.05^{22}\}, \tag{21}$$

where λ is the wavelength. The above spacings were chosen so that the array had the same aperture as a 24-element ULA with an interelement spacing of $\frac{1}{2}\lambda$.

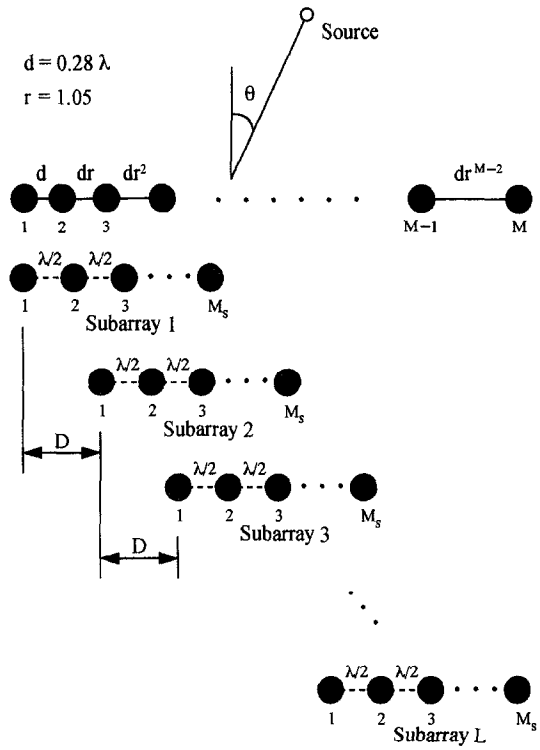

Fig. 1. Geometry of real array and virtual subarrays in nonuniform linear array case.

The array was interpolated into $L = 8$ virtual linear subarrays, each having M_s elements equally spaced by $\frac{1}{2}\lambda$. As depicted in Fig. 1, these subarrays were uniformly placed within the aperture of the real array. Setting the reference point at the first element of the real array, the direction vectors associated with the real array and ith virtual subarrays are given by

$$\boldsymbol{a}(\theta) = \left[1, \mathrm{e}^{\mathrm{j}\frac{2\pi d}{\lambda}\sin\theta}, \mathrm{e}^{\mathrm{j}\frac{2\pi d}{\lambda}(1+r)\sin\theta}, \ldots, \mathrm{e}^{\mathrm{j}\frac{2\pi d}{\lambda}\frac{r^{(M-1)}-1}{r-1}\sin\theta}\right]^{\mathrm{T}},$$

$$\boldsymbol{b}_i(\theta) = \mathrm{e}^{\mathrm{j}\left(\frac{M-M_s}{L-1}\right)\pi(i-1)\sin\theta} \times \left[1, \mathrm{e}^{\mathrm{j}\pi\sin\theta}, \mathrm{e}^{\mathrm{j}2\pi\sin\theta}, \ldots, \mathrm{e}^{\mathrm{j}(M_s-1)\pi\sin\theta}\right]^{\mathrm{T}}, \tag{22}$$

where $d = 0.28\lambda$, $r = 1.05$, and the angle variable θ is measured with respect to the broadside of the array.

The primary and auxiliary interpolation regions were chosen as

$$\Theta = [-3°, 3°] \cup [-45°, -35°] \cup [20°, 40°], \quad (23)$$

with $\Theta_D = [-3°, 3°]$ and

$$\Theta_A = [-90°, -45°] \cup [-35°, -10°] \cup [10°, 20°] \cup [40°, 90°]. \quad (24)$$

Firstly, Figs. 2(a) and (b) show the TRIE value for the regular and SD interpolators, respectively, as a function of M_s, with ε as a variable parameter. The TRIE is observed to be stable with respect to M_s, and increase with ε. This coincides with our observation regarding the weighting effect of ε on the interpolation performance. Next, Figs. 2(c) and (d) show the LRIE as a function of θ with $M_s = 12$, and ε as a variable parameter. Comparing the interpolation error within the primary and auxiliary regions gives an indication as to how the trade-off of interpolation performance between the two regions is achieved with a suitable ε. The interpolator with $\varepsilon = 0$ exhibits excessively large errors over Θ_A, which is incurred with the ill-condition problem. In this case, $\varepsilon = 10^{-4}$ gives an interpolation error on the order of 10^{-4}, and should be an adequate choice for the scenario considered [9]. In fact, we found that selecting an ε value less than 10^{-4} did not give any noticeable improvement.

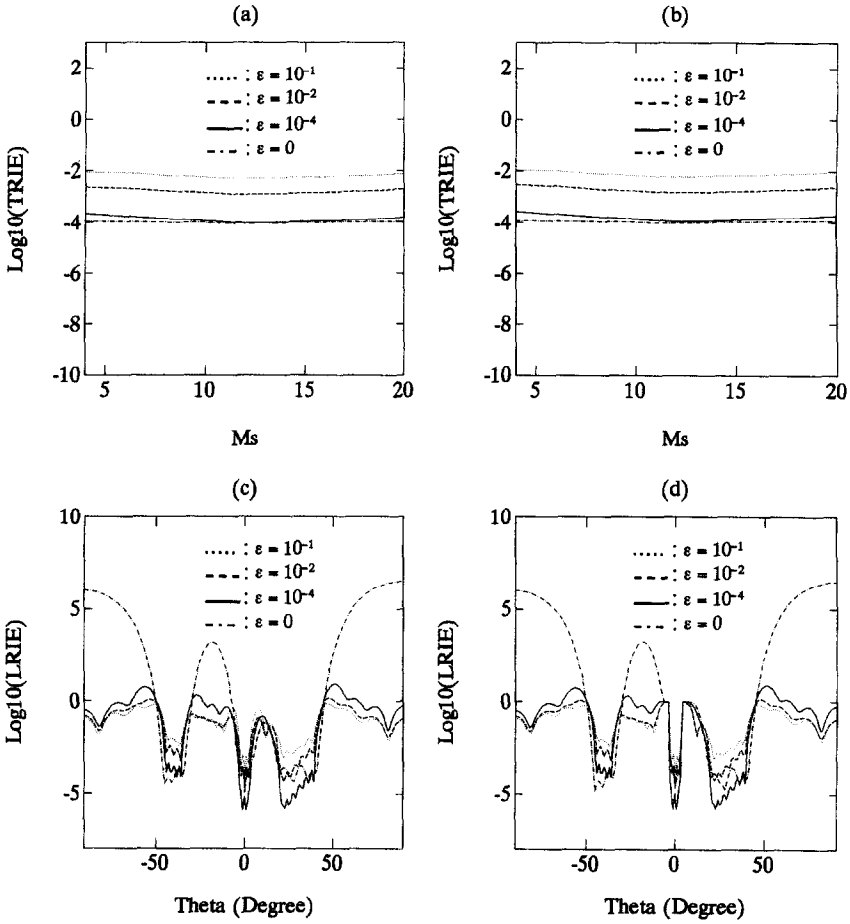

Fig. 2. (a), (b): Total relative interpolation error as a function of M_s, with ε as a variable parameter. $M = 24$, $L = 8$. (a) Regular type; (b) SD type. (c), (d): Local relative interpolation error as a function of θ, with ε as a variable parameter. $M = 24$, $M_s = 12$ and $L = 8$. (c) Regular type; (d) SD type. Linear array case.

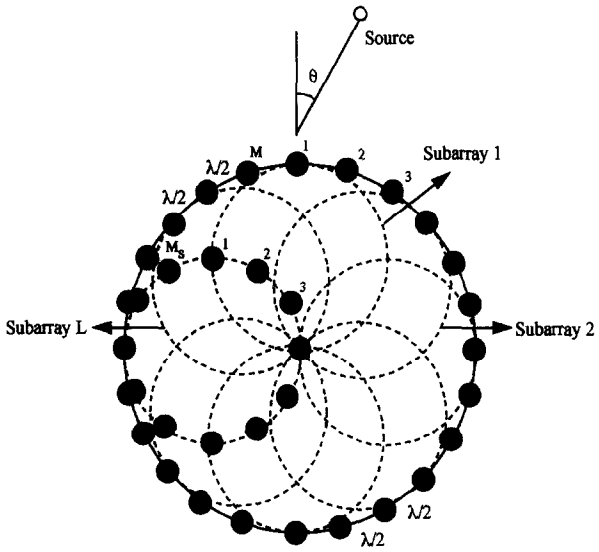

Fig. 3. Geometry of real array and virtual subarrays in the circular array case.

The example was repeated with a 24-element circular array with radius R. The elements, assumed all identical and omnidirectional, were equally spaced by $\frac{1}{2}\lambda$ such that $R \approx 1.91\lambda$. The array was interpolated into $L = 8$ virtual circular subarrays, each having M_s elements equally spaced by $\frac{1}{2}\lambda$. These virtual subarrays were placed uniformly on a circle within the aperture of the real array, as illustrated in Fig. 3. Setting the reference point at the center of the real array, the direction vectors associated with the real array and ith virtual subarrays are given by

$$\boldsymbol{a}(\theta) = \left[e^{j\frac{2\pi R}{\lambda}\cos\theta}, e^{j\frac{2\pi R}{\lambda}\cos(\theta-\frac{2\pi}{M})}, \ldots, e^{j\frac{2\pi R}{\lambda}\cos(\theta-\frac{2(M-1)\pi}{M})}\right]^T,$$

$$\boldsymbol{b}_i(\theta) = e^{j\frac{2\pi(R-R_s)}{\lambda}\cos(\theta-\frac{2(i-1)\pi}{L})} \times \left[e^{j\frac{2\pi R_s}{\lambda}\cos\theta}, e^{j\frac{2\pi R_s}{\lambda}\cos(\theta-\frac{2\pi}{M_s})}, \ldots, e^{j\frac{2\pi R_s}{\lambda}\cos(\theta-\frac{2(M_s-1)\pi}{M_s})}\right]^T, \quad (25)$$

where $R_s = \lambda/(4\sin(\pi/M_s))$ is the radius of the virtual subarrays. In this case, we assume that all the sources are confined on the array plane such that the elevation angle is always zero, and θ is the azimuth angle. The primary and auxiliary interpolation regions were chosen as

$$\Theta = [-5°, 5°] \cup [-87.5°, -72.5°] \cup [40°, 70°], \quad (26)$$

with $\Theta_D = [-5°, 5°]$ and

$$\Theta_A = [-180°, -87.5°] \cup [-72.5°, -20°] \cup [20°, 40°] \cup [70°, 180°]. \quad (27)$$

Fig. 4 shows the TRIE and LRIE curves for both types of interpolators corresponding to Fig. 2. Again $M_s = 12$ was chosen for computing the LRIE. The same trend as in the previous case is observed regarding the interpolation performance with respect to ε. We note that in contrast to the linear array case, $\varepsilon = 0$ gives significantly better interpolation performance over Θ than other values. However, this is achieved at the cost of excessively large errors over Θ_A. In this case, $\varepsilon = 10^{-4}$ gives an interpolation error on the order of 10^{-5}, and should be a more than adequate choice for the scenario considered.

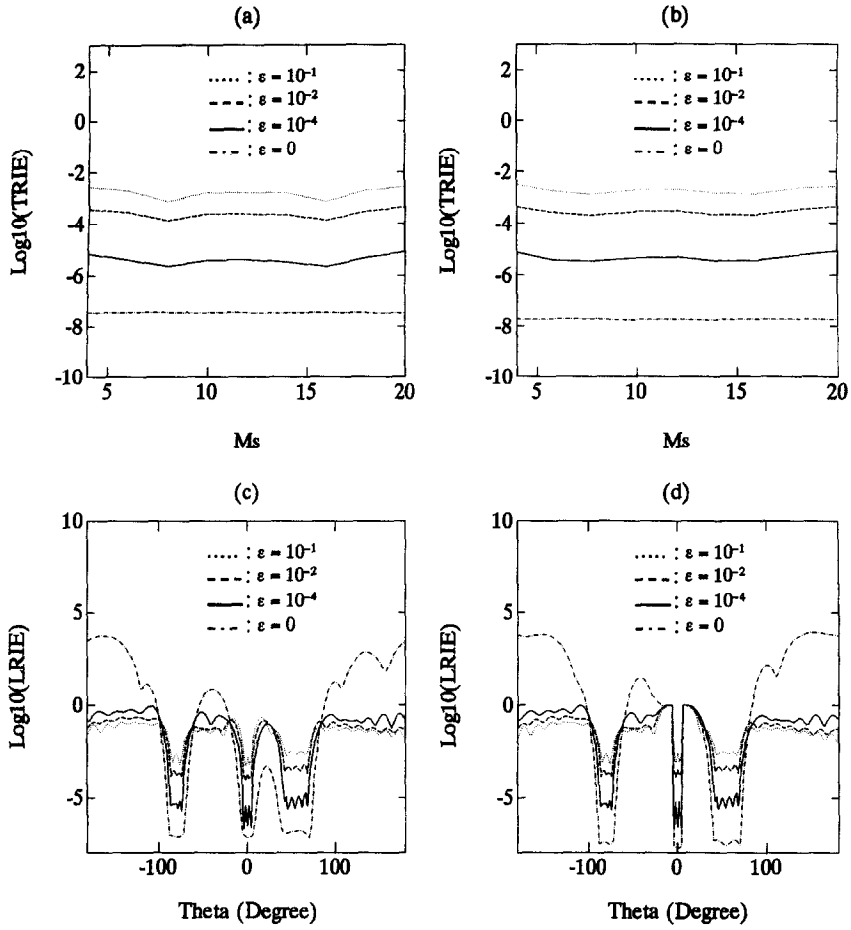

Fig. 4. (a), (b): Total relative interpolation error as a function of M_s, with ε as a variable parameter. $M=24$, $L=8$. (a) Regular type; (b) SD type. (c), (d): Local relative interpolation error as a function of θ, with ε as a variable parameter. $M=24$, $M_s=12$ and $L=8$. (c) Regular type; (d) SD type. Circular array case.

4. Construction of optimum beamformer

This section describes the procedure for constructing the beamformer with interpolated subarrays. The procedure involves two stages:

1. Obtain the optimum subarray weight vector based on spatially smoothed virtual subarray correlation matrix.
2. Convert the optimum subarray weight vector back into a full aperture weight vector for the real array.

4.1. Stage 1. Optimum subarray beamformer

If the interpolator works well, the real array will be mapped into L nearly identical virtual subarrays. On these subarrays we observe the transformed SD data according to Eqs. (1) and (9):

$$\tilde{\boldsymbol{x}}_i = \tilde{\boldsymbol{T}}_i \boldsymbol{x} \approx \tilde{\boldsymbol{B}}_i \tilde{\boldsymbol{s}} + \tilde{\boldsymbol{T}}_i \boldsymbol{n}, \quad i=1,\ldots,L, \tag{28}$$

where

$$\tilde{\boldsymbol{B}}_i = [\boldsymbol{b}_i(\theta_1), \boldsymbol{b}_i(\theta_2), \ldots, \boldsymbol{b}_i(\theta_K)], \quad i=1,\ldots,L, \tag{29}$$

and $\tilde{\boldsymbol{s}} = [s_1, s_2, \ldots, s_K]^{\mathrm{T}}$. These data are called the SD data because they contain essentially no desired signal. Since the virtual subarrays are identical except for a spatial displacement, they are related through

$$\tilde{\boldsymbol{B}}_i = \tilde{\boldsymbol{B}}_s \boldsymbol{\Phi}_i, \quad i=1,\ldots,L, \tag{30}$$

where $\tilde{\boldsymbol{B}}_s$ is associated with a 'reference' subarray (i.e., $\tilde{\boldsymbol{B}}_s = \tilde{\boldsymbol{B}}_i$ if the ith subarray is chosen as the reference), and

$$\boldsymbol{\Phi}_i = \begin{bmatrix} e^{j\phi_i(\theta_1)} & & & \boldsymbol{0} \\ & e^{j\phi_i(\theta_2)} & & \\ & & \ddots & \\ \boldsymbol{0} & & & e^{j\phi_i(\theta_K)} \end{bmatrix}, \quad i = 1, \ldots, L, \tag{31}$$

with $\phi_i(\theta)$ being the phase shift between the ith and reference subarrays induced by a wavefront from direction θ.

The optimum subarray beamforming weight vector, denoted as $\boldsymbol{w}_s$, is determined via the LCMV problem described in (5):

$$\min_{\boldsymbol{w}_s} \quad \boldsymbol{w}_s^H \bar{\boldsymbol{R}} \boldsymbol{w}_s$$

$$\text{subject to} \quad \boldsymbol{w}_s^H \boldsymbol{b}_s(\theta_0) = 1, \tag{32}$$

where $\boldsymbol{b}_s(\theta)$ is the direction vector associated with the reference subarray, and $\bar{\boldsymbol{R}}$ is the $M_s \times M_s$ spatially smoothed virtual subarray correlation matrix given according to Eqs. (6), (28) and (30) by

$$\bar{\boldsymbol{R}} = \frac{1}{L}\sum_{i=1}^{L} E\{\tilde{\boldsymbol{x}}_i \tilde{\boldsymbol{x}}_i^H\} = \frac{1}{L}\sum_{i=1}^{L} \tilde{\boldsymbol{T}}_i \boldsymbol{R}_{xx} \tilde{\boldsymbol{T}}_i^H$$

$$\approx \frac{1}{L}\sum_{i=1}^{L} \tilde{\boldsymbol{B}}_i \tilde{\boldsymbol{R}}_{ss} \tilde{\boldsymbol{B}}_i^H + \sigma_n^2 \frac{1}{L}\sum_{i=1}^{L} \tilde{\boldsymbol{T}}_i \tilde{\boldsymbol{T}}_i^H$$

$$= \tilde{\boldsymbol{B}}_s \bar{\boldsymbol{R}}_{ss} \tilde{\boldsymbol{B}}_s^H + \sigma_n^2 \bar{\boldsymbol{Q}}, \tag{33}$$

where $\tilde{\boldsymbol{R}}_{ss} = E\{\tilde{\boldsymbol{s}}\tilde{\boldsymbol{s}}^H\}$ is the SD source correlation matrix, and

$$\bar{\boldsymbol{R}}_{ss} = \frac{1}{L}\sum_{i=1}^{L} \boldsymbol{\Phi}_i \tilde{\boldsymbol{R}}_{ss} \boldsymbol{\Phi}_i^H \tag{34}$$

and

$$\bar{\boldsymbol{Q}} = \frac{1}{L}\sum_{i=1}^{L} \tilde{\boldsymbol{T}}_i \tilde{\boldsymbol{T}}_i^H \tag{35}$$

represent the effective SD source correlation matrix and noise correlation matrix, respectively, observed on the spatially smoothed virtual subarray. It is the averaging operation in Eq. (34) that destroys the coherence among the interferers. Problem (32), which is similar in structure to (5), has the solution

$$\boldsymbol{w}_s = \gamma_s \bar{\boldsymbol{R}}^{-1} \boldsymbol{b}_s(\theta_0), \tag{36}$$

where γ_s is a normalizing scalar.

4.2. Stage 2. Dimension recovery for full array weight vector

As long as the condition of degree of freedom is satisfied, the resulting 'master' subarray beamformer constructed with $\boldsymbol{w}_s$ will produce a unit gain at θ_0 and a deep null in each of the K interference directions such that

$$\boldsymbol{w}_s^H \boldsymbol{b}_s(\theta_0) = 1,$$

$$\boldsymbol{w}_s^H \boldsymbol{b}_s(\theta_k) \approx 0, \quad k = 1, \ldots, K. \tag{37}$$

We refer to this virtual beamformer as the 'interference cancellation' (IC) beamformer. If the regular type interpolation is adequately performed in (8), we have

$$\boldsymbol{T}_i \boldsymbol{a}(\theta_k) \approx \boldsymbol{b}_i(\theta_k) = e^{j\phi_i(\theta_k)} \boldsymbol{b}_s(\theta_k),$$

$$k = 0, 1, \ldots, K, \; i = 1, \ldots, L, \tag{38}$$

such that

$$(\boldsymbol{T}_i^H \boldsymbol{w}_s)^H \boldsymbol{a}(\theta_0) \approx e^{j\phi_i(\theta_0)} \boldsymbol{w}_s^H \boldsymbol{b}_s(\theta_0) = e^{j\phi_i(\theta_0)},$$

$$(\boldsymbol{T}_i^H \boldsymbol{w}_s)^H \boldsymbol{a}(\theta_k) \approx e^{j\phi_i(\theta_k)} \boldsymbol{w}_s^H \boldsymbol{b}_s(\theta_k) \approx 0,$$

$$k = 0, 1, \ldots, K, \; i = 1, \ldots, L. \tag{39}$$

This says that the set of weight vectors

$$\boldsymbol{w}_i = e^{j\phi_i(\theta_0)} \boldsymbol{T}_i^H \boldsymbol{w}_s, \quad i = 1, \ldots, L, \tag{40}$$

acting on the real array will produce a unit gain at θ_0 and nulls in each of the interference directions. In other words, the look direction gain and interference nulls has been translated to $\boldsymbol{w}_i$, $i = 1, \ldots, L$, on the real array. The reason for using $\boldsymbol{T}_i$'s here instead of $\tilde{\boldsymbol{T}}_i$'s is thus evident since $\tilde{\boldsymbol{T}}_i$ cannot retain the look direction gain of $\boldsymbol{w}_s$. The 'back transformation' in (40) is similar in principle to the copying of weights from the master beamformer to the slave beamformer as described in Ref. [11]. However, a distinctive feature in Eq. (40)

is that multiple slave beamforming weight vectors are available.

The full array weight vectors $\boldsymbol{w}_i$, $i=1,\ldots,L$, can be regarded as a set of 'basis' vectors for the construction of the real array weight vector. A question now arises as to how the L basis vectors should be combined into a single weight vector. The problem may be described as finding an $L \times 1$ combining coefficient vector $\boldsymbol{g}=[g_1, g_2, \ldots, g_L]^{\mathrm{T}}$ such that the combined weight vector

$$\boldsymbol{w}=\sum_{i=1}^{L} g_i \boldsymbol{w}_i = \boldsymbol{W}\boldsymbol{g} \tag{41}$$

exhibits a certain optimality, where

$$\boldsymbol{W}=[\boldsymbol{w}_1, \boldsymbol{w}_2, \ldots, \boldsymbol{w}_L]. \tag{42}$$

The block diagram illustrating the synthesis and operation of the beamformer is given in Fig. 5. Note that it is the combined weight vector $\boldsymbol{w}$ that acts on the real array data $\boldsymbol{x}$ to produce to beamformer output y. The following sections describe two types of combiners.

4.2.1. Maximum output SNR (MSNR) combiner

If the basis weight vectors cancel the interference well, then the output due to the combined weight vector will contain essentially the desired signal and noise only. This is because that any linear combination of $\boldsymbol{w}_i$, $i=1,\ldots,L$, will also cancel the interference. A reasonable criterion for choosing $\boldsymbol{g}$ in this case would be to maximize the output SNR of the resulting full array beamformer. This leads to the following problem:

$$\max_{\boldsymbol{g}} \frac{E\{|\boldsymbol{g}^{\mathrm{H}}\boldsymbol{W}^{\mathrm{H}}\boldsymbol{a}(\theta_{\mathrm{d}})s_{\mathrm{d}}|^2\}}{E\{|\boldsymbol{g}^{\mathrm{H}}\boldsymbol{W}^{\mathrm{H}}\boldsymbol{n}|^2\}}$$

$$= \frac{E\{|s_{\mathrm{d}}|^2\}}{\sigma_n^2} \frac{\boldsymbol{g}^{\mathrm{H}}\boldsymbol{W}^{\mathrm{H}}\boldsymbol{a}(\theta_{\mathrm{d}})\boldsymbol{a}^{\mathrm{H}}(\theta_{\mathrm{d}})\boldsymbol{W}\boldsymbol{g}}{\boldsymbol{g}^{\mathrm{H}}\boldsymbol{W}^{\mathrm{H}}\boldsymbol{W}\boldsymbol{g}}. \tag{43}$$

With the unknown θ_{d} replaced by the look direction θ_0, we obtain the following equivalent problem:

$$\min_{\boldsymbol{g}} \quad \boldsymbol{g}^{\mathrm{H}}\boldsymbol{W}^{\mathrm{H}}\boldsymbol{W}\boldsymbol{g}$$

$$\text{subject to} \quad \boldsymbol{g}^{\mathrm{H}}\boldsymbol{W}^{\mathrm{H}}\boldsymbol{a}(\theta_0)=1, \tag{44}$$

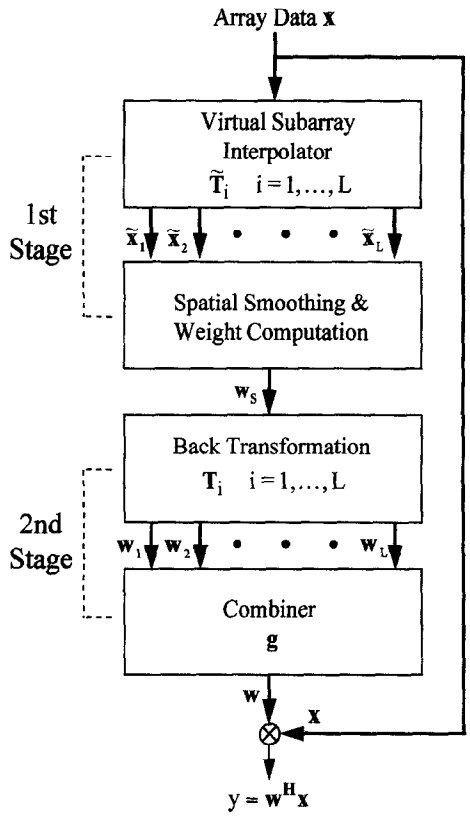

Fig. 5. Block diagram of two-stage interpolated beamformer.

which is again an LCMV problem whose solution is given by

$$\boldsymbol{g}=\gamma_g(\boldsymbol{W}^{\mathrm{H}}\boldsymbol{W})^{-1}\boldsymbol{W}^{\mathrm{H}}\boldsymbol{a}(\theta_0), \tag{45}$$

where again γ_g is a normalizing scalar.

It is interesting to note that the full array weight vector obtained by substituting Eq. (45) into (41),

$$\boldsymbol{w}=\gamma_g\boldsymbol{W}(\boldsymbol{W}^{\mathrm{H}}\boldsymbol{W})^{-1}\boldsymbol{W}^{\mathrm{H}}\boldsymbol{a}(\theta_0), \tag{46}$$

can be interpreted algebraically as the orthogonal projection of $\boldsymbol{a}(\theta_0)$ onto the range space of $\boldsymbol{W}$. This makes sense since $\boldsymbol{a}(\theta_0)$ is the optimum weight vector which maximizes the beamformer output SNR under the quiescent (spatially white noise only) condition. On the other hand, the range space of $\boldsymbol{W}$ represents the 'subspace of interference cancellation'. Projecting $\boldsymbol{a}(\theta_0)$ orthogonally onto the range space of $\boldsymbol{W}$ is tantamount to finding a vector lying in the subspace of

interference cancellation which is closest to the optimum quiescent weight vector.

The inversion of $\boldsymbol{W}^{\mathrm{H}}\boldsymbol{W}$ in (45) dictates that $\boldsymbol{W}$ cannot be ill-conditioned in order to avoid numerical problems. Making $\boldsymbol{W}$ well-conditioned is equivalent to making the vectors $\boldsymbol{w}_i$, $i=1,\ldots,L$, well separated. This implies from (40) that the transformation matrices $\boldsymbol{T}_i$, $i=1,\ldots,L$, should be well separated as well. Since these matrices are directly related to the virtual subarray configuration, it is conceived that a set of spatially well separated virtual subarrays will give the desired $\boldsymbol{W}$. This is another reason for restricting the subarray number L in addition to that mentioned earlier in Section 3.1.

4.2.2. Eigen-based combiner

The MSNR combiner inherently assumes that θ_0 is accurate enough so that the real array pattern $w(\theta)$ will exhibit a mainlobe pointed at the desired source. In the presence of a large pointing error, however, it cannot guarantee a satisfactory reception of the desired signal due to the beam squint problem. This necessitates a technique with which the computation of weight vectors is independent of θ_0. In Ref. [2], a method based on the eigenvalue decomposition (EVD) was proposed to extract the 'signal subspace' from a transformed correlation matrix with the interference removed. The signal subspace is represented by an eigenvector producing a large gain in the desired source direction. We now demonstrate that the same technique can be readily applied to the combiner discussed herein.

Consider the real array beamformer output as expressed by

$$\begin{aligned}\boldsymbol{w}^{\mathrm{H}}\boldsymbol{R}_{xx}\boldsymbol{w} &= \boldsymbol{g}^{\mathrm{H}}\boldsymbol{W}^{\mathrm{H}}\boldsymbol{R}_{xx}\boldsymbol{W}\boldsymbol{g}\\ &\approx E\{|s_{\mathrm{d}}|^2\}|\boldsymbol{g}^{\mathrm{H}}\boldsymbol{W}^{\mathrm{H}}\boldsymbol{a}(\theta_{\mathrm{d}})|^2+\sigma_n^2\boldsymbol{g}^{\mathrm{H}}\boldsymbol{W}^{\mathrm{H}}\boldsymbol{W}\boldsymbol{g},\end{aligned} \tag{47}$$

where we have used Eq. (6) and the fact that the interference has been eliminated by $\boldsymbol{W}$ (i.e., $\boldsymbol{W}^{\mathrm{H}}\boldsymbol{a}(\theta_k)\approx \boldsymbol{0}_L$, $k=1,\ldots,K$). With pointing errors present, the beamformer response $\boldsymbol{g}^{\mathrm{H}}\boldsymbol{W}^{\mathrm{H}}\boldsymbol{a}(\theta_{\mathrm{d}})$ is not known. In this case, the optimum beamformer can be determined as one that maximizes the signal-plus-noise-to-noise ratio (SNNR). In other words, the coefficient vector $\boldsymbol{g}$ is determined in accordance with

$$\max_{\boldsymbol{g}}\frac{\boldsymbol{g}^{\mathrm{H}}\boldsymbol{W}^{\mathrm{H}}\boldsymbol{R}_{xx}\boldsymbol{W}\boldsymbol{g}}{\boldsymbol{g}^{\mathrm{H}}\boldsymbol{W}^{\mathrm{H}}\boldsymbol{W}\boldsymbol{g}}. \tag{48}$$

By maximizing the total output power with the noise power fixed, we have in fact forced the beamformer to produce a large gain for the desired signal. Let $\boldsymbol{u}_i$, $i=1,\ldots,L$, be the generalized eigenvectors (GEV's) satisfying

$$\boldsymbol{W}^{\mathrm{H}}\boldsymbol{R}_{xx}\boldsymbol{W}\boldsymbol{u}_i=\xi_i\boldsymbol{W}^{\mathrm{H}}\boldsymbol{W}\boldsymbol{u}_i,\quad i=1,\ldots,L, \tag{49}$$

where $\xi_1\geqslant\xi_2\geqslant\cdots\geqslant\xi_L$, are the corresponding generalized eigenvalues (Gev's) arranged in descending order. The solution to (48) is given by $\boldsymbol{g}=\boldsymbol{u}_1$, the GEV associated with the largest Gev. By choosing $\boldsymbol{w}$ to be

$$\boldsymbol{w}=\gamma_g\boldsymbol{W}\boldsymbol{u}_1, \tag{50}$$

the beamformer will automatically produce a mainlobe peak near θ_{d}.

It should be mentioned that the efficacy of the eigen-based combiner lies in that the interference has been suppressed sufficiently by the virtual subarray beamformer constructed with $\boldsymbol{w}_{\mathrm{s}}$, and that the transformation has successfully translated the interference nulls from $\boldsymbol{w}_{\mathrm{s}}$ to each of $\boldsymbol{w}_i$'s. Otherwise, any residual interfering power left in $\boldsymbol{W}^{\mathrm{H}}\boldsymbol{R}_{xx}\boldsymbol{W}$ will be likely stronger than the desired signal power and thus cause confusion in maximizing the SNNR by the leading GEV.

5. Simulation results

Computer simulations were conducted to ascertain the performance of the proposed two-stage interpolated beamformer. Specifically, the performance of the beamformer was examined against spatially white noise, pointing errors and deviations of interpolation region. For all cases, we assumed that the data correlation matrices involved in computing the optimum weight vectors were available, and did not concern ourselves with the problem of estimating them.

5.1. Part 1. Linear array case

In this case, the 24-element linear array and the associated subarray configuration as described in Section

3.5 were employed. For all cases, the real array was interpolated into $L = 8$ uniform linear virtual subarrays of size $M_s = 12$. The desired source was at $\theta_d = 0°$, and $K = 3$ interferers were generated at $\theta_1 = -40°$, $\theta_2 = 28°$ and $\theta_3 = 33°$. The source correlation matrix was set to be

$$\boldsymbol{R}_{ss} = \begin{bmatrix} 1 & 0 & 0 & 0 \\ 0 & 1000 & 0 & 0 \\ 0 & 0 & 100 & 100 \\ 0 & 0 & 100 & 100 \end{bmatrix}, \tag{51}$$

which means that the second and third interferers are coherent with the same power corresponding to a signal-to-interference ratio (SIR) of -20 dB, and the first interferer is uncorrelated with the other three sources with an SIR of -30 dB. As an evaluation index, we define the beamformer output SINR as

$$\mathrm{SINR}_0 = \frac{E\{|s_d|^2\}|\boldsymbol{w}^H\boldsymbol{a}(\theta_d)|^2}{\sum_{i=1}^{3}\sum_{k=1}^{3}\boldsymbol{R}_{ss}(i+1,k+1)\boldsymbol{w}^H\boldsymbol{a}(\theta_i)\boldsymbol{a}^H(\theta_k)\boldsymbol{w} + \sigma_n^2\boldsymbol{w}^H\boldsymbol{w}}. \tag{52}$$

The first set of examples evaluates the performance of the interpolated beamformer against white noise. In this case, the correct look direction $\theta_0 = 0°$ was used (no pointing error). The primary and auxiliary interpolation regions were the same as those given in Eqs. (23) and (24), respectively. Fig. 6(a) shows the curves of SINR_0 versus input SNR for different values of ε obtained with the MSNR type of combiner. For comparison, we also include the maximum possible output SINR (M times the input SNR) obtained with the optimum quiescent beamformer. We find that the beamformer performs better as ε decreases, and the trend is the same for all input SNR values. This is consistent with the result that a small ε leads to a small interpolation error. The SINR_0 values obtained with $\varepsilon = 10^{-4}$ are close to the optimum ones, indicating that the second stage combiner was effective in boosting up the output SNR. It is noteworthy that the beamformer remains reliable with an SNR as low as -10 dB. This confirms that the drop in beamforming gain due to the interpolation error is negligible as compared to the signal/interference level. As a demonstration, we show in Fig. 6(b) the beam pattern $w(\theta)$ obtained with SNR = 10 dB and $\varepsilon = 10^{-4}$. The corresponding subarray pattern $w_s(\theta)$ is also included for comparison. We observe that three deep nulls are located in the interference directions for both $w(\theta)$ and $w_s(\theta)$, indicating that these nulls were successfully generated by the subarray beamformer and then translated to the full array beamformer. It is noteworthy that the second and third interferers are separated by approximately half the 3-dB beamwidth of the subarray ($\approx 9.6°$).

The second set of simulations examines the effects of pointing errors on the proposed beamformer. In this case, the look direction θ_0 was varied from $-5°$ to $5°$, corresponding to a maximum pointing error of $5°$ (the 3-dB beamwidth of the array is approximately $4.8°$). The input SNR was fixed at 10 dB, and the other parameters were the same as in the previous simulation. Figs. 7(a) and (b) show the curves of SINR_0 versus θ_0 for different values of ε. Both types of combiners were tested for comparison. The results indicate that desired signal cancellation did not occur with pointing errors (no performance breakdown). The MSNR combiner exhibits a certain degradation in performance due to the beam squint effect. The eigen-based combiner, on the other hand, is surprisingly robust. These are confirmed by the beam patterns shown in Figs. 7(c) and (d) obtained with $\theta_0 = -5°$ and $\varepsilon = 10^{-4}$. Clearly, both combiners successfully cancelled the three interferers even with a large pointing error. Moreover, the eigen-based combiner was able to 'resteer' the beam back to the desired source direction to compensate for the pointing error at the first stage. This did not happen with the MSNR combiner.

The final set of simulations examines the effects of deviations of the interpolation region. In this case, the primary interpolation region was modified into

$$\Theta = [-3°, 3°] \cup [-45° + \Delta\theta, -35° + \Delta\theta] \cup [20°, 40°], \tag{53}$$

with $-10° \leqslant \Delta\theta \leqslant 10°$, and Θ_A was modified accordingly. This corresponds to a maximum deviation of

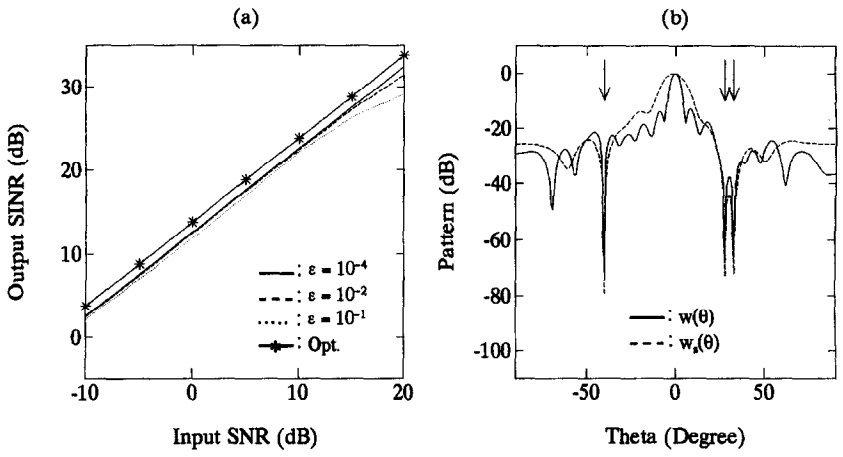

Fig. 6. (a) Comparison of beamformer output SINR versus input SNR with ε as a parameter. (b) Beam patterns obtained with input SNR = 10 dB and $\varepsilon = 10^{-4}$. $\theta_d = 0°$, $\theta_1 = -40°$, $\theta_2 = 28°$ and $\theta_3 = 33°$. $\theta_0 = 0°$. Linear array case.

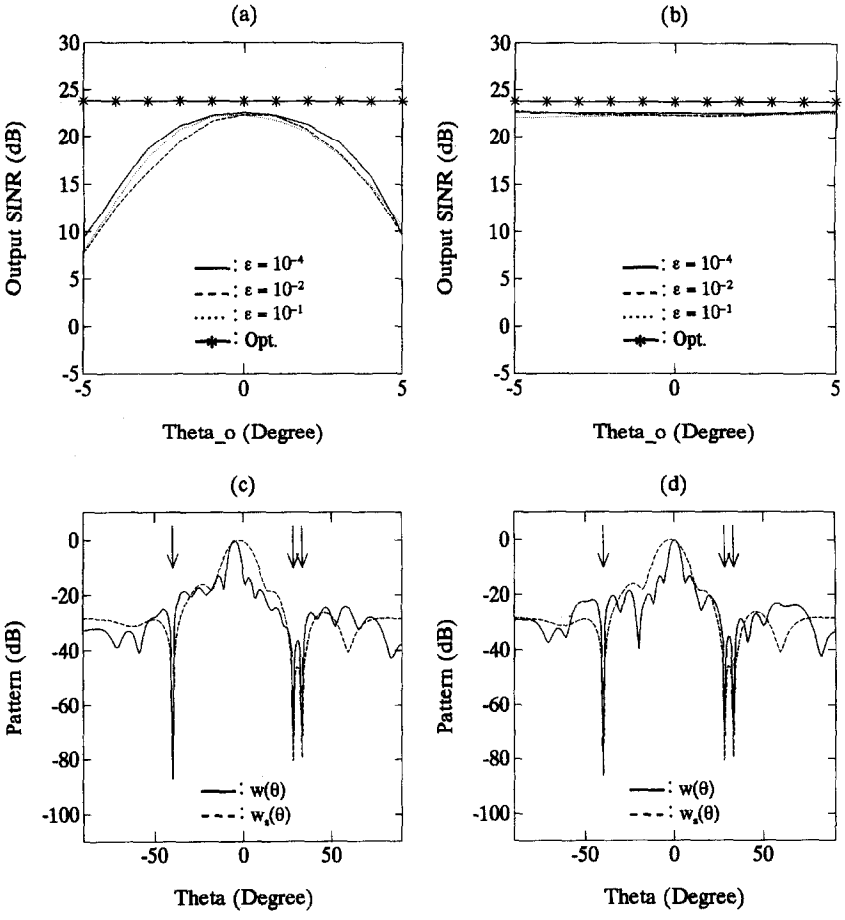

Fig. 7. (a), (b): Comparison of beamformer output SINR versus pointing error with ε as a parameter. (a) MSNR combiner; (b) eigen-based combiner. (c), (d): Beam patterns obtained with $\theta_0 = -5°$ and $\varepsilon = 10^{-4}$. (c) MSNR combiner; (d) eigen-based combiner. $\theta_d = 0°$, $\theta_1 = -40°$, $\theta_2 = 28°$ and $\theta_3 = 33°$. Input SNR = 10 dB. Linear array case.

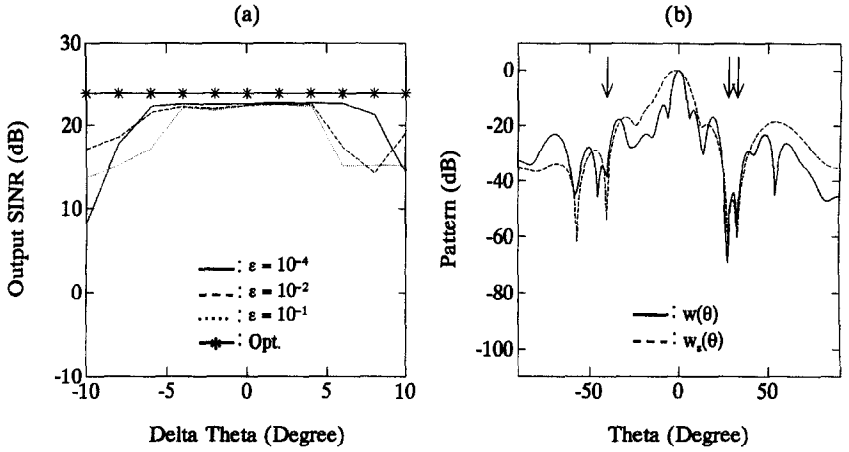

Fig. 8. (a) Comparison of beamformer output SINR versus deviation of one interpolation region with ε as a parameter. (b) Beam patterns obtained with $\Delta\theta = -10°$ and $\varepsilon = 10^{-4}$. $\theta_d = 0°$, $\theta_1 = -40°$, $\theta_2 = 28°$ and $\theta_3 = 33°$. $\theta_0 = 0°$. Input SNR = 10 dB. Linear array case.

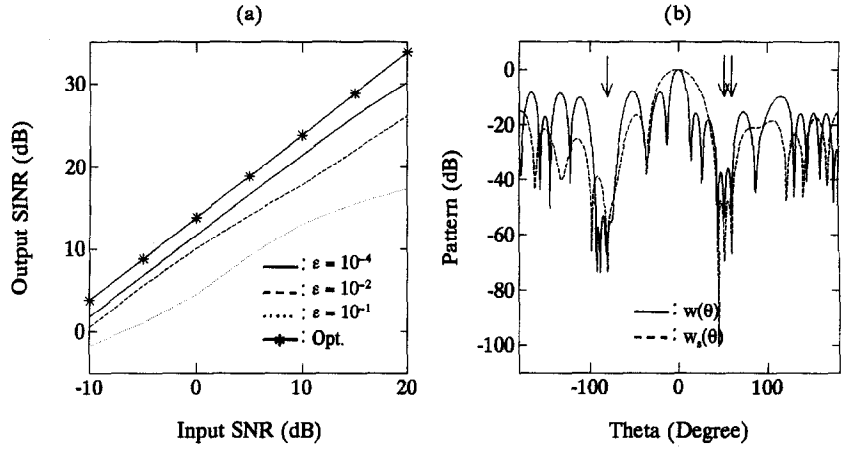

Fig. 9. (a) Comparison of beamformer output SINR versus input SNR with ε as a parameter. (b) Beam patterns obtained with input SNR = 10 dB and $\varepsilon = 10^{-4}$. $\theta_d = 0°$, $\theta_1 = -80°$, $\theta_2 = 52°$ and $\theta_3 = 60°$. $\theta_0 = 0°$. Circular array case.

10° in choosing the interpolation region associated with the first interferer. Again the input SNR was fixed at 10 dB, and the other parameters were the same as in the first simulation. Fig. 8(a) plots the resulting $SINR_0$ curves versus $\Delta\theta$ for different values of ε obtained with the MSNR combiner. The beamformer is observed to perform reasonably well for $-5° \leqslant \Delta\theta \leqslant 5°$. Outside that region its performance is not reliable but still acceptable even when the interpolator fails to operate for the first interferer (for $|\Delta\theta| > 5°$). This is an indication of the 'extrapolation' capability of the interpolator. To gain more insights, we show in Fig. 8(b) the beam patterns obtained with $\Delta\theta = -10°$ and $\varepsilon = 10^{-4}$. We note that although the first interferer was not perfectly cancelled, the beamformer was still able to impose sufficient attenuation on it to prevent performance breakdown. On the other hand, the other two interferers were eliminated as desired without being affected by the large deviation angle.

5.2. *Part 2. Circular array case*

In this subsection, we repeat the three sets of simulation work in Part 1 with the 24-element circular array

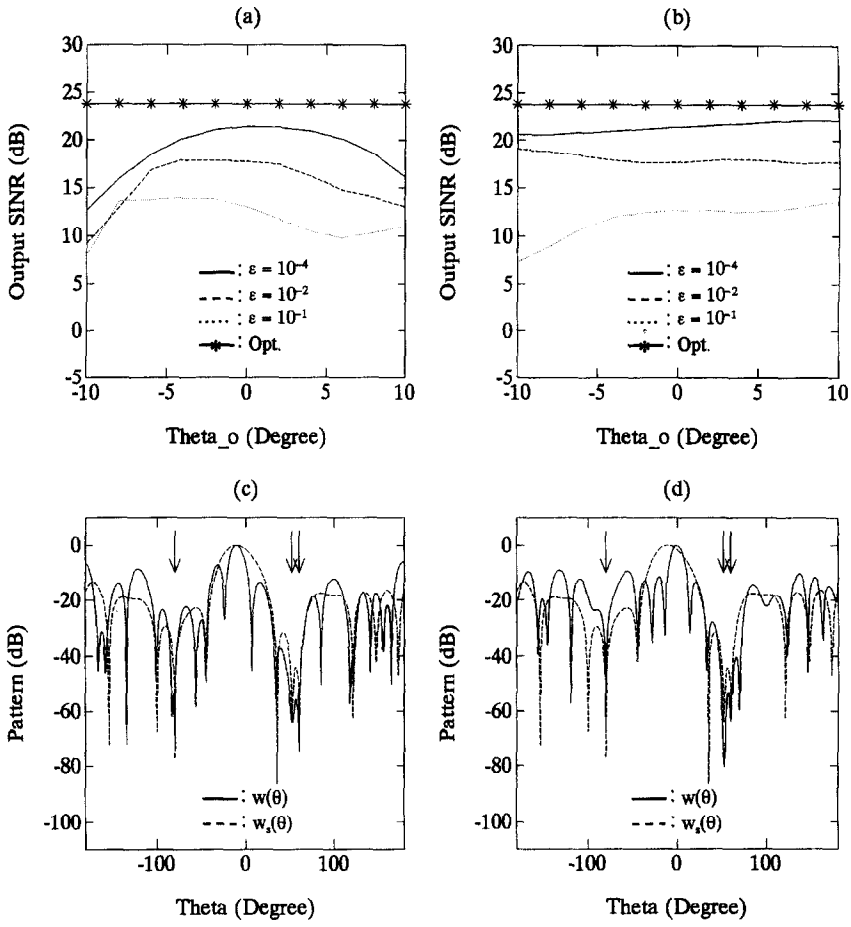

Fig. 10. (a), (b): Comparison of beamformer output SINR versus pointing error with ε as a parameter. (a) MSNR combiner; (b) eigen-based combiner. (c), (d): Beam patterns obtained with $\theta_0 = -10°$ and $\varepsilon = 10^{-4}$. (c) MSNR combiner; (d) eigen-based combiner. $\theta_d = 0°$, $\theta_1 = -80°$, $\theta_2 = 52°$ and $\theta_3 = 60°$. Input SNR = 10 dB. Circular array case.

described in Section 3.5. For all cases, the real array was interpolated into $L = 8$ virtual circular subarrays of $M_s = 12$ elements with the configuration depicted in Fig. 3. The desired source was at $\theta_d = 0°$, and $K = 3$ interferers were generated at $\theta_1 = -80°$, $\theta_2 = 52°$ and $\theta_3 = 60°$. The source correlation matrix was the same as (51).

The first set of examples evaluates the performance of the interpolated beamformer against white noise. Again, the correct look direction $\theta_0 = 0°$ was used, and the primary and auxiliary interpolation regions were the same as those given in Eqs. (26) and (27), respectively. Fig. 9(a) shows the curves of $SINR_0$ versus input SNR obtained with the MSNR type combiner. The results follow the same trend as observed in the linear array case, except that the disparity in performance associated with different ε values is more significant than that observed in Fig. 6(a). Also, the $SINR_0$ values are not as close to the optimum ones as in the linear array case. We have tried smaller ε but found no noticeable improvement. Choosing a larger M_s will slightly increase the output SINR, but the price is a rise in complexity. A careful examination on the two-stage behaviors of the beamformer reveals that, although the subarray beamformer successfully cancelled the interference, the second stage combiner was not able to recover the full SNR gain capability of the real array. This is deemed as the cost of imposing the

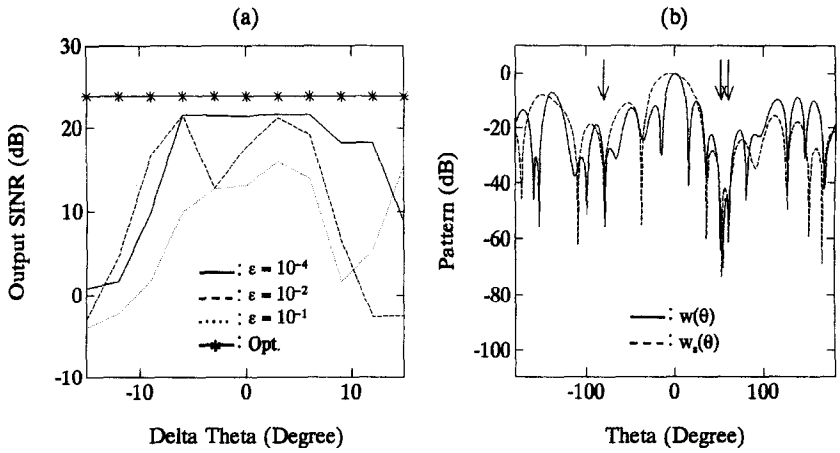

Fig. 11. (a) Comparison of beamformer output SINR versus deviation of one interpolation region with ε as a parameter. (b) Beam patterns obtained with $\Delta\theta = -15°$ and $\varepsilon = 10^{-4}$. $\theta_d = 0°$, $\theta_1 = -80°$, $\theta_2 = 52°$ and $\theta_3 = 60°$. $\theta_0 = 0°$. Input SNR $= 10$ dB. Circular array case.

two-stage scheme on the circular array. The beam pattern obtained with SNR $= 10$ dB and $\varepsilon = 10^{-4}$ is given in Fig. 9(b) along with the corresponding subarray pattern. Three deep nulls are found in the interference directions for both $w(\theta)$ and $w_s(\theta)$, as in the linear array case.

The second set of simulations examines the effects of pointing errors. The look direction θ_0 was varied from $-10°$ to $10°$, corresponding to a maximum pointing error of $10°$. The input SNR was fixed at 10 dB, and the other parameters were the same as in the previous simulation. Figs. 10(a) and (b) show the curves of SINR_0 versus θ_0 for different values of ε obtained with both types of combiners. The results are similar in trend to those observed in Figs. 7(a) and (b). Again, the disparity among the curves is more significant than in the linear array case. Figs. 10(c) and (d) show the corresponding beam patterns obtained with $\theta_0 = -10°$ and $\varepsilon = 10^{-4}$. The results are quite similar in nature to those observed in Figs. 7(c) and (d).

The final set of simulations examines the effects of deviations of the interpolation region. In this case, the primary interpolation region was modified into

$$\Theta = [-5°, 5°] \cup [-87.5° + \Delta\theta, -72.5° + \Delta\theta] \cup [40°, 70°], \tag{54}$$

with $-15° \leqslant \Delta\theta \leqslant 15°$, and Θ_A was modified accordingly. This corresponds to a maximum deviation of $15°$ in choosing the interpolation region associated with the first interferer. The input SNR was fixed at 10 dB, and the other parameters were the same as in the first simulation. Fig. 11(a) shows the resulting SINR_0 curves versus $\Delta\theta$ for different values of ε obtained with the MSNR combiner. We see that the beamformer performs well with $\varepsilon = 10^{-4}$ as long as the interference direction is contained in the interpolation region (for $|\Delta\theta| \leqslant 7.5°$). For other ε values, the beamformer was not as reliable in the presence of deviations. Finally the beam patterns obtained with $\Delta\theta = -15°$ and $\varepsilon = 10^{-4}$ confirm that the interpolator does indeed exhibit a certain extrapolation effect outside its operation region. The first interferer (SIR $= -30$ dB) received a gain of approximately -30 dB, resulting in an output SINR close to 0 dB.

6. Conclusions

A method of adaptive beamforming in the presence of multiple coherent interferers was presented which can be applied to arbitrary array geometry. The beamformer was developed based on interpolation, spatial smoothing and dimension recovery. The interpolator transformed the real array into several identical virtual subarrays with the desired signal removed. A spatially smoothed virtual subarray was then formed with the interferers decorrelated, on which the

optimum subarray beamformer was constructed. By a judiciously designed procedure, we successfully converted the subarray beamformer back into a full aperture beamformer for the original array. The full array beamformer preserves the interference nulls of the subarray beamformer and optimizes the output signal–noise condition. In particular, two types of combiners were suggested for dimension recovery: the maximum SNR combiner and the eigen-based combiner. We showed that the eigen-based combiner gave better performance if the interferers were sufficiently suppressed in the subarray beamformer. Numerical examples confirmed that the output SINR performance of the proposed two-stage beamformer is quite reliable as long as the interpolation error is confined to a moderate size. For the linear array case, the proposed beamformer can perform almost as well as the optimum beamformer working under the quiescent situation.

Acknowledgements

This work was supported by the National Science Council of R.O.C. under Grant NSC 85-2213-E-009-017.

References

[1] B. Friedlander, "The root-MUSIC algorithm for direction finding with interpolated arrays", *Signal Processing*, Vol. 30, No.1, January 1993, pp. 15–29.

[2] J.W. Kim and C.K. Un, "An adaptive array robust to beam pointing error", *IEEE Trans. Signal Process.*, Vol. 40, No. 6, January 1991, pp. 76–84.

[3] C.C. Ko, "Robust algorithm for combating look direction error problems", *IEEE Trans. Aerosp. Electron. Syst.*, Vol. 31, No. 3, July 1995, pp. 1043–1052.

[4] J.H. Lee and J.F. Wu, "Adaptive beamforming without signal cancellation in the presence of coherent jammers", *IEE Proc.-F*, Vol. 136, No. 4, August 1989, pp. 169–173.

[5] A.K. Luthra, "A solution to adaptive nulling problem with a look-direction constraint in the presence of coherent jammers", *IEEE Trans. Antennas Propagat.*, Vol. 34, No. 5, May 1986, pp. 702–710.

[6] R.A. Monzingo and T.W. Miller, *Introduction to Adaptive Arrays*, Wiley, New York, NY, 1980, Chapter 1, pp. 3–21.

[7] S.C. Pei, C.C. Yeh and S.C. Chiu, "Modified spatial smoothing for coherent jammer suppression without signal cancellation", *IEEE Trans. Acoust. Speech Signal Process.*, Vol. 36, No. 3, March 1988, pp. 412–414.

[8] T.J. Shan and T. Kailath, "Adaptive beamforming for coherent signals and interference", *IEEE Trans. Acoust. Speech Signal Process.*, Vol. 33, No. 6, June 1985, pp. 527–536.

[9] B.D. Van Veen and K.M. Buckly, "Beamforming: A versatile approach to spatial filtering", *IEEE ASSP Mag.*, April 1988, pp. 4–24.

[10] A.J. Weiss and B. Friedlander, "Performance analysis of spatial smoothing with interpolated arrays", *IEEE Trans. Signal Process.*, Vol. 41, No. 5, May 1993, pp. 1881–1892.

[11] B. Widrow, K.M. Duvall, R.P. Gooch and W.C. Newman, "Signal cancellation phenomena in adaptive antennas: Causes and cures", *IEEE Trans. Antennas Propagat.*, Vol. 30, No. 5, May 1982, pp. 469–478.

[12] C.C. Yeh and W.D Wang, "Coherent interference suppression by an antenna array of arbitrary geometry", *IEEE Trans. Antennas Propagat.*, Vol. 37, No. 10, October 1989, pp. 1317–1322.